TOPICAL REVIEW — Amorphous physics and materials

Amorphous phase formation rules in high-entropy alloys*

Qiu-Wei Xing(邢秋玮) and Yong Zhang(张勇)†

State Key Laboratory for Advanced Metals and Materials, University of Science and Technology Beijing, Beijing 100083, *China*

(Received 12 September 2016; revised manuscript received 2 November 2016; published online 8 December 2016)

There have been many interesting studies on high-entropy alloys (HEAs), also known as multi-component (MC) alloys (MCAs), in recent years. MC metallic-glasses (MGs) have shown the potential to express the advantages of MCAs and MGs in tandem. Amorphous phase formation rules are a crucial issue in the HEA and MCA field. For equal or near-equal atomic ratio alloys, mixed-entropy among the elements has a significant effect on the phase formation. This paper focuses on HEA amorphous phase formation rules. In the first two sections, the recent progress in amorphous phase formation in HEAs and MCAs is reviewed, including the effective factors and correlative parameters related to amorphous phase formation. In the third section, novel MCMGs including high-entropy (HE) bulk-metallic-glass (HE-BMG) and MCMG films developed in recent decades are summarized, and the giant-magnetic-impedance (GMI) effect of MC amorphous fibers is discussed.

Keywords: high-entropy alloys, bulk metallic glasses, amorphous phase, fiber materials

PACS: 81.05.Bx, 81.05.Kf, 81.05.Zx, 81.30.Bx **DOI:** 10.1088/1674-1056/26/1/018104

1. Introduction

Since first reported in 2003,[1] multi-component (MC) alloys (MCAs) have garnered attention across a variety of research fields. Initially,[2–4] MCAs were constituted of five or more elements with equal or near equal atomic concentration, and usually formed into simple solid solution phases with body-centered cubic (BCC), face-centered cubic (FCC), or hexagonal closed-packed (HCP) structure. Yeh *et al.*[2] proposed that the high configurational entropy of the alloys stabilizes the disordered random-solid-solution phase structure, thus this series of alloys are also referred to as high-entropy alloys (HEAs). Alongside the development of non-equal atomic ratio HEAs[5,6] and high-entropy (HE) metallic glasses (MGs) in recent decades,[7–10] the entropy of some alloys is lower than the maximum value calculated by the ideal mixture equation. As opposed to the traditional alloys, the compositions of MCAs are normally located near the center of their diagrams (not the edges or corners). By virtue of their unique compositions and microstructures, MCAs tend to have remarkable, novel properties compared to the traditional alloys.[11,12]

Metallic bonding is omnidirectional and unsaturated, so metallic atoms tend to form simple close-packed structures with three-dimensional periodicity. Their crystalline structure gives the metallic material anisotropy and a stable melting point. Unlike normal metallic materials, metallic glasses (MGs) have a long-range disordered structure. A series of MGs with good glass-forming abilities (GFA) have been discovered[13] since the first Au-Si MGs ribbons were fabricated via rapid solidification in 1960.[14] MGs normally have higher strength, higher elastic strain limits, higher corrosion resistance, and higher wear resistance than the alloys with similar composition. Compared to oxide glasses, atoms of MGs rely on metallic bonding to combine with each other, the characteristics of metals, such as electrical conductivity, are well-retained in MGs.

Over past several years, amorphous phase formation has been widely investigated as a component of phase selection rules in MCAs.[15] Although MCAs mostly form intermetallics, complex phases, and (occasionally) solid-solution phases, ordered or disordered, in a few cases they may form amorphous phase.[16] A new type of bulk metallic glasses (BMGs) known as high-entropy (HE) metallic-glasses (HE-BMGs) have been developed under the guidance of this novel alloy design strategy. HE-BMGs have greatly expanded the scope of MGs.

In this article, we review the amorphous formation in MCAs and summarize notable achievements in MCMGs field. Effective factors in regards to amorphous phase in MCAs are discussed in Section 2. The established formation rules, including correlative parameters and phase diagrams, based on the effective factors are reviewed in Section 3. Finally, novel MCMGs, with special focus on the HE-BMGs with good GFA, MCA films with non-crystalline structure, and the GMI effect of MC amorphous micro-fibers, are discussed in Section 4.

2. Effective factors on amorphous phase formation in MCAs

Liquid metal can be super-cooled far below the equilibrium melting temperature without crystallization.[17] The first

*Project supported by the National Natural Science Foundation of China (Grant No. 51471025).

†Corresponding author. E-mail: drzhangy@ustb.edu.cn

© 2017 Chinese Physical Society and IOP Publishing Ltd

MGs ever discovered, usually with a limited size, must be solidified at very high cooling rate (over 10^6 K/s) to suppress crystallization during processing. In 1990s, Inoue developed a series of bulk-metallic glasses (BMGs) with large GFA in MCA systems.[18–21] $Zr_{41.2}Cu_{12.5}Ni_{10}Ti_{13.8}Be_{22.5}$BMG (vit-1), which was discovered by Johnson,[22] can form glass under the critical cooling rate of 1 K/s. To date, BMGs have been explored in Zr-, Cu-, Fe-, Pd-, Ni-, Mg-, Ti-, and rare-earth-based (RE-based) alloy systems; the critical size of BMG can reach 73 mm in diameter.[13,23]

Inoue proposed three empirical rules related to the common features of MGs with large GFA:[24] 1) The alloy system contains at least three elements. 2) The mixing enthalpy among the principle elements has a large and negative value. 3) The atomic size difference among the major constituent elements is larger than 12%. The first rule is in accordance with the MCA design strategy. Although these empirical rules are not applicable for all alloy systems, they are essential guidelines for the BMG alloy design. In addition, a number of indicated criteria have been established to measure the GFA of BMGs, for instance, reduced glass-transition temperature T_{rg} ($T_{rg} = T_g/T_l$),[17] super-cooled liquid region width ΔT_x ($\Delta T_x = T_x - T_g$),[25] and parameter γ ($\gamma = T_x/(T_g + T_l)$),[26] etc. These criteria can reflect relative GFA among BMGs.

In addition to the empirical rules and criteria mentioned above, the mixing entropy is a requisite factor to be considered in amorphous phase formation. The following section discusses the effects of the mixing entropy, mixing enthalpy, atomic size, and amorphous phase formation rules in MCAs.

2.1. Effect of entropy on amorphous phase formation in MCAs

A greater number of components increase the likelihood of glass formation – this is known as the "confusion principle", which was first proposed by Greer.[27] Based on the confusion principle, alloys constituted by more than three elements always have high GFA. Though the confusion principle does not explicitly give the necessary concentration of each element for glass formation, it is logical to infer that high mixing entropy could raise the GFA in MCAs. MCA fabrication scenarios are not always identical to those of BMGs, however; for example, an alloy consisting of 20 different components forms a multi-crystal mixture instead of expected amorphous phase.[28] The Gibbs phase rule comes into play here as well. It can be expressed as follows (at constant pressure):

$$F + P = C + 1, \tag{1}$$

where F is the number of degrees of freedom, C is the number of components, and P is the number of phases in thermodynamic equilibrium with each other. Equation (1) indicates that the maximum phase number in condensed systems can reach $C + 1$.

Interestingly, subsequent experiments confirmed that certain equal atomic alloys such as $Fe_{20}Cr_{20}Ni_{20}Mn_{20}Co_{20}$ can form a single solid solution with FCC structure,[28] and $Co_{20}Cr_{20}Fe_{20}Ni_{20}Al_{20}$ alloys can form a solid solution with BCC structure.[29] Single-phase hexagonal close-packed (HCP) structure was also discovered in YGdTbDyLu and GdTbDyTmLu alloys.[30] Extensive research has demonstrated that the phase number of MCAs is usually much lower than the maximum number indicated by the Gibbs phase rule. The stability of the solid solution phase in MCAs is due to the HE effect.[2] For a regular solution, the configurational entropy of mixing in MCAs can be calculated via the ideal mixtures equation

$$\Delta S_{\text{mix}} = -R\sum_{i=1}^{n}(c_i \ln c_i), \tag{2}$$

where c_i is the mole percent of the i-th component in the alloy system, and R ($= 8.314$ J·K^{-1}·mol^{-1}) is the gas constant. According to Eq. (2), the configurational entropy of mixing reaches its maximum in equal-atomic ratio alloys. MCAs possess unique structures when the configurational entropy of mixing is more than $1.61R$.[31] It is crucial to account for the fact that the HE of mixing usually restrains glass formation in MCAs, however. This fact can be supported by the Adams-Gibbs equation

$$\eta = \eta_0 \cdot \exp\frac{C}{T\Delta S_{\text{mix}}(T)}, \tag{3}$$

where η is the actual viscosity, η_0 is the ideal viscosity, C is the activation energy barrier to cooperative arrangements, T is the temperature, and ΔS_{mix} is the configurational entropy. Of course, the viscosity declines with increasing configurational entropy. Decrease in viscosity is conducive to atomic migration in alloy melts and reduced GFA in MCAs.

2.2. Effect of enthalpy on amorphous phase formation in MCAs

Glass formers usually have large and negative mixing enthalpy among the major elements, which, as-reflected in the phase diagrams, characterizes their deep eutectics.[16] Moreover, the liquid temperature T_l of a glass former is usually close to the glass-transition temperature T_g at or near the eutectic point in the phase diagram. Turnbull[17] proposed reduced glass transition temperature T_{rg} ($T_{rg} = T_g/T_l$) to measure the GFA of alloys accordingly. MCAs can be regarded as good glass formers when $T_{rg} > 0.6$, however, the effect of the initial crystallization temperature T_x is not indicated in parameter T_{rg}. BMGs typically have a large super-cooled liquid region ΔT_x ($\Delta T_x = T_x - T_g$),[25] meaning that T_g should be far below the initial crystallization temperature T_x. By synthesizing both factors, parameter $\gamma(\gamma = T_x/(T_g + T_l))$ is more accurate than T_{rg} and ΔT_x in the judgment of GFA.[26]

When the number of major elements is more than five, it is difficult to ensure large and negative mixing enthalpy between the elements. The enthalpy of mixing for a MCA system can be calculated as follows:[32]

$$\Delta H_{\rm mix}=\sum_{i=1,i\neq j}^{n}4\Omega_{ij}c_ic_j, \tag{4}$$

where $\Omega_{ij}(=\Delta H_{\rm mix}AB)$ is the regular solution interaction parameter between the i-th and the j-th elements, and $\Delta H_{\rm mix}AB$ is the enthalpy of mixing for the binary equal atomic AB alloys consisted of the i-th and the j-th components, which is given by Ref. [13]. c_i and c_j are the mole percentages of the i-th and the j-th components, respectively.

2.3. Effect of atomic size on amorphous phase formation in MCAs

The atomic distributions of MGs and MCAs are both random in the alloy matrix. Moreover, MG has a long-range disordered structure. Greer proposed that "confusion" element will be different from each other by size.[27] Inoue identified atomic size difference larger than 12%, and Senkov[33] found that some atoms are located in interstitial sites while others substitute for matrix atoms as a result of significant atomic size difference. Both kinds of atoms are configured in a short-range ordered structure in MCMGs, thus playing a stabilizing role in amorphous phase formation. The topological dense packing structure of atoms raises the viscosity of alloy melts. High viscosity decreases the atomic distribution, impedes the nucleation and growth of grains, and enhances the GFA in MCAs.[31]

Atomic size difference in MCAs is usually measured by parameter δ, which can be expressed as follows:

$$\delta=\sqrt{\sum_{i=1}^{n}c_i\left(1-\frac{r_i}{\bar{r}}\right)^2}, \tag{5}$$

$$\bar{r}=\sum_{i=1}^{n}c_ir_i, \tag{6}$$

where $\bar{r}$ is the average atomic radius, and c_i and r_i are the atomic percentage and atomic radius of the i-th component, respectively.

From the perspective of entropy, Takeuchi *et al.*[34] correlated parameter δ with mismatch entropy S_δ, and revealed $S_\delta/k_{\rm B}\sim(\delta/22)^2$, where $k_{\rm B}$ is the Boltzmann constant. When the atomic size difference is small, S_δ can be ignored. A given BMG system usually has a significant atomic size difference, and thus significant atomic size mismatch, so S_δ must be considered together with the configurational entropy $\Delta S_{\rm mix}$ to determine the phase formation in MCAs.

3. Amorphous phase formation rules in MCAs

None of the thermodynamics parameters mentioned above can solely control the MCA phase formation. It is necessary to consider the combination of an array of factors to accurately predict the amorphous phase formation in MCAs. As a basic thermodynamic equation, the Gibbs-Helmholtz equation readily describes the correlation between enthalpy and entropy of the system.

In a MCA system, the mixing Gibbs free energy is expressed as follows:

$$\Delta G_{\rm mix}=\Delta H_{\rm mix}-T\Delta S_{\rm mix}. \tag{7}$$

As a result of large component number and equal atomic ratio, the effect of the mixing entropy is an important part of MCAs phase formation. Amorphous phase formation is determined by competition between mixing enthalpy $\Delta H_{\rm mix}$ and $\Delta S_{\rm mix}$.

In consideration of the competition between ordering and disordering processes in BMGs, Xia *et al.*[35] proposed the concept of rearrangement-inhibiting ability to reflect the GFA of BMGs. The concept is simplified as parameter ε, which is calculated as follows:

$$\varepsilon=-\frac{\Delta S_{\rm mix}}{\Delta H_{\rm mix}}, \tag{8}$$

where $\Delta S_{\rm mix}$ is expressed differently from that in Eq. (2)

$$\Delta S_{\rm mix}=-R\sum_{i=1}^{n}c_i\ln\varphi_i, \tag{9}$$

$$\varphi_i=\frac{c_ir_i^3}{\sum_{i=1}^{n}c_ir_i^3}. \tag{10}$$

Here r_i is the atomic radius, so the atomic size difference is also taken into account in parameter ε. The amorphous phase formation range is approximately restricted within $0.25\ {\rm K}^{-1}<\varepsilon<0.6\ {\rm K}^{-1}$. As opposed to other GFA criteria (ΔT_x, $T_{\rm g}$, and γ), parameter ε can be calculated prior to alloy fabrication. Its efficiency has been confirmed in Tb–Fe–Al ternary alloys.

It is important to note that compared to Eq. (7), melting temperature $T_{\rm m}$ is not considered in ε. Further, taking the configurational entropy, mixing enthalpy, and atomic radius into one parameter makes the expression of ε somewhat complex. When applied in MCAs, the competition between $\Delta H_{\rm mix}$ and $\Delta S_{\rm mix}$ can be described by[36]

$$\Omega=\frac{T_{\rm m}\Delta S_{\rm mix}}{|\Delta H_{\rm mix}|}, \tag{11}$$

where mixing enthalpy $\Delta H_{\rm mix}$ and mixing entropy $\Delta S_{\rm mix}$ can be calculated by Eqs. (2) and (4), respectively. $T_{\rm m}$ is the melting temperature of MCAs, which can be estimated by the law of mixtures

$$T_{\rm m}=\sum_{i=1}^{n}c_i(T_{\rm m})_i, \tag{12}$$

where $(T_{\rm m})_i$ is the melting point of the i-th alloy component.

In Eq. (11), when $\Omega>1$, $T_{\rm m}\Delta S_{\rm mix}$ exceeds $\Delta H_{\rm mix}$ as the predominant component of free energy. On the contrary,

the enthalpy of mixing becomes dominant in phase formation when $\Omega < 1$. When using two or three parameters to predict amorphous phase formation, the relationship among parameters can be drawn as a 2D or 3D diagram. The relationship between Ω and δ of MCAs is depicted as an example in Fig. 1. Clearly, the stable solid-solution phase forms when $\Omega > 1.1$ and $\delta < 6.6\%$. The "BMG" zone marked in the figure indicates where an amorphous phase forms when Ω is small and δ is large.[36]

In addition to the Ω–δ diagram, the $\Delta H_{\rm mix}$–δ diagram (Fig. 2)[37] is generally used to identify solid solution formation zones in intermetallic and BMGs – especially when the effect of $\Delta S_{\rm mix}$ is less obvious. As shown in Fig. 2, solid solution formed alloys cluster in the zone marked S and S′, and amorphous phase formed alloys distribute in the zones marked B_1 and B_2. Amorphous phases tend to form under the condition of larger δ and negative $\Delta H_{\rm mix}$. If considering $\Delta S_{\rm mix}$ as a third parameter, the $\Delta S_{\rm mix}$–$\Delta H_{\rm mix}$–δ diagram can be drawn into a three-dimensional graph.

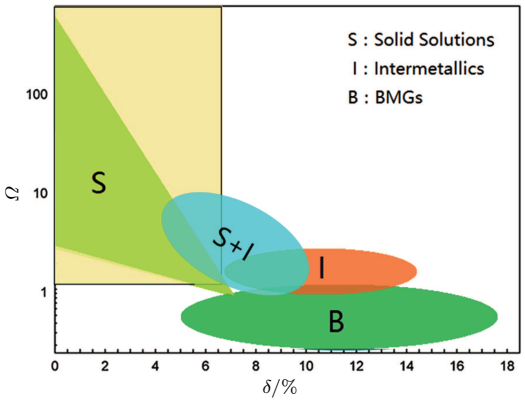


Fig. 1. (color online) Relationship between parameters Ω and δ for MCAs, Solid solution indicates the alloy containing only solid solution; intermetallics indicate the alloy mainly containing intermetallic compounds and other ordered phases; S + I indicates solid solution formation in addition to the ordered compound precipitation in MCAs; and BMGs indicate that the alloy can form amorphous phases. The figure is reproduced from Ref. [36].

Guo *et al.*[38] utilized $\Delta H_{\rm mix}$ and atomic size difference δ to identify the MCA amorphous phase formation and found that a solid solution can form when $\delta <\sim 6.6\%$ and $\sim 11.6 < \Delta H_{\rm mix} < 3.2$ kJ/mol. MCAs located at the red region of the $\Delta H_{\rm mix}$–δ diagram ($\Delta H_{\rm mix} \leq -12.2$ kJ/mol, $\delta \geq 6.4\%$) can form amorphous phases, as shown in Fig. 3. δ is the critical parameter, and $\delta = 6.5\%$ is a good criterion to distinguish the formation of solid solutions and amorphous phases.

Takeuchi *et al.*[34] proposed that mismatch entropy S_δ is an essential factor when the atomic difference is large. Based on the relationship $S_\delta/k_{\rm B} \sim (\delta/22)^2$, they suggested that a $\Delta H_{\rm mix}$–δ^2 diagram can be utilized to predict MCA amorphous phase formation. A comparison can be made between $\Delta H_{\rm mix}$–δ (Fig. 1) and $\Delta H_{\rm mix}$–δ^2 (Fig. 4) diagrams. The purple zone in either diagram marks the amorphous phase formation region, while the blue zone indicates the solid solution formation region. The phase formation regions of both diagrams are similar and correlated with each other.

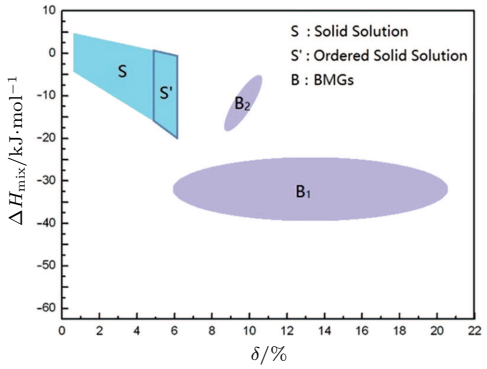


Fig. 2. (color online) Relationship between δ and $\Delta H_{\rm mix}$ for MCAs. Solid solution indicates that the alloy contains only solid solutions, ordered solid solution indicates minor-ordered solid solution precipitates besides the solid solution, and BMGs indicate that the alloy can form amorphous phases. The figure is reproduced from Ref. [37].

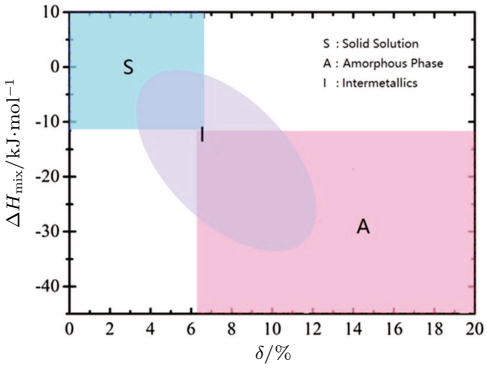


Fig. 3. (color online) $\Delta H_{\rm mix}$–δ plot delineating the phase selection in MCAs. The figure is reproduced from Ref. [38].

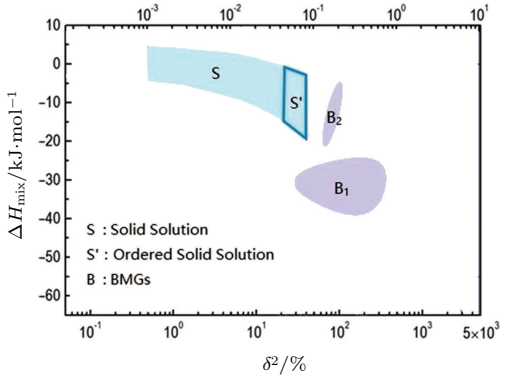


Fig. 4. (color online) $\Delta H_{\rm mix}$–δ^2 diagrams, containing solid solution, ordered solid solution, and BMG information. The figure is reproduced from Ref. [34].

According to the literature, $\Delta H_{\rm mix}$, $\Delta S_{\rm mix}$, and δ are effective parameters to predict amorphous phase formation. When extended to non-equal atomic alloys and alloys with fewer elements, $\Delta H_{\rm mix}$ and δ become two major parameters to be considered. Several recent investigations have indicated, however, that the atomic radius difference is the vital factor in determining MCA phase formation.

Previous studies have shown that δ generally reveals the average effect of atomic size difference in the alloy system, but does not provide a geometrical relationship or structural details between different atoms.[39] As a result, δ is not particularly useful in managing the transitional zone from the solid solution to the BMG. In diagrams with δ, intermetallic and multiple phases usually exist in both solid solution and BMG regions, especially near the junction of the two regions (Figs. 1 and 3).

In a binary solid solution, component elements are divided into solute and solvent elements. The relationship between atomic size difference and local structure can be illustrated under the Hume–Rothery rule. When extended to MCAs, the boundary between solute and solvent elements is not nearly as clear. Egami[40] built a local packing model for MGs and proposed the volume strain as a criterion to judge the topological instability of the dense random packing structure. The concept of atomic level stresses also provides means to understand the local structure of MGs.[41]

Wang *et al.*[39] suggested using γ to replace δ based on the atomic packing model. Parameter γ is the ratio between the solid angles of the smallest and the largest atoms, which can be expressed as follows:

$$\gamma=\frac{\omega_{\mathrm{S}}}{\omega_{\mathrm{L}}}, \tag{13}$$

$$\omega_{\mathrm{L}}=1-\sqrt{\frac{(r_{\mathrm{L}}+\bar{r})^2-\bar{r}^2}{(r_{\mathrm{L}}+\bar{r})^2}}, \tag{14}$$

$$\omega_{\mathrm{S}}=1-\sqrt{\frac{(r_{\mathrm{S}}+\bar{r})^2-\bar{r}^2}{(r_{\mathrm{S}}+\bar{r})^2}}, \tag{15}$$

where r_{L} and r_{S} are the largest and the smallest atomic radii, respectively, so ω_{L} and ω_{S} respectively represent the solid angles around the largest and the smallest atoms. Compared to δ, the physical meaning of γ is clearer, $\gamma=1.175$ as a dividing line can effectively identify solid solutions from intermetallics. In this way, amorphous phases are all distributed in the region of $\gamma>1.175$, but do not have clear boundaries against intermetallics.

Ye *et al.*[42] used the following root mean square (R.M.S.) residual strain to state the relationship between dense packing and phase transition:

$$\left\langle \varepsilon^2 \right\rangle^{1/2}=\sqrt{\sum_{i=j}^{n} c_j \varepsilon_j^2}, \tag{16}$$

where ε_j is the instinct residual strain of the j-th atom. The $\Delta H_{\mathrm{mix}}-\left\langle \varepsilon^2 \right\rangle^{1/2}$ diagram (Fig. 5) can facilitate a clear comparison between mixed enthalpy and R.M.S. residual strain. When projected to the axis of ΔH_{mix}, different zones have relatively large overlapped regions. The situation is obviously better on the horizontal axis. An amorphous structure forms when the R.M.S. residual strain is larger than 10%. Compared to other criteria, superposition zones between three phase formation regions are relatively few; thus $\left\langle \varepsilon^2 \right\rangle^{1/2}$ is better suited to identifying amorphous phases from single-phase solid solutions and multiple phases.

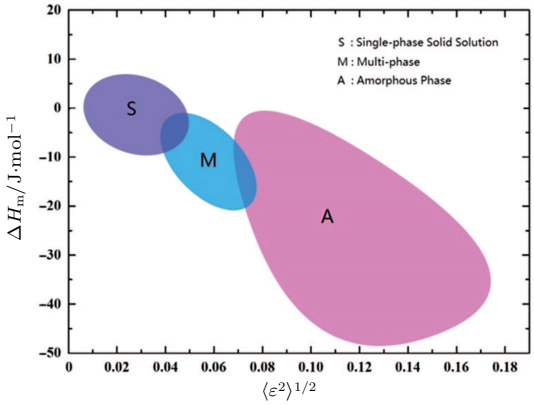


Fig. 5. (color online) ΔH_{mix}–$\langle \varepsilon^2 \rangle^{1/2}$ diagram for HEAs and BMGs. The figure is reproduced from Ref. [42].

The formation rules mentioned above are far from perfectly suited to phase prediction and are indeed ineffective in some cases. For example, Takeuchi[43] manufactured $Ti_{20}Zr_{20}Pd_{20}Cu_{20}Ni_{20}$ metallic-glass ribbons under high cooling rate (melt-spinning method), then after adding 0.5 at% Al, $Al_{0.5}$TiZrPdCuNi satisfied two conditions of glass formation ($\Delta H_{\mathrm{mix}}=-46.7$ kJ·mol^{-1} and $\delta=8\%$); the $Al_{0.5}$TiZrPdCuNi abnormally formed a solid solution phase with BCC structure instead of the expected amorphous phase though the alloy is far from the solid solution zone in the ΔH_{mix}–δ^2 diagram. The cause of this conversion from amorphous phase to solid solution phase remains unclear. In addition, certain predictive parameters require modification for low-density MCAs – especially in alloys containing Al, Li, or Mg.[44] The electronegativity difference ($\Delta\chi$) and valence electron concentration (VEC) also play crucial roles in MCA phase selection, though their impact on amorphous phase formation is less obvious.[45] There are a number of unknown zones yet to be explored.

4. Multi-component metallic-glasses

Unlike conventional MGs, MCMGs normally have equal or near equal molar ratio among elements. In addition, as the application of amorphous phase formation rules in MCAs, MCMGs not only have good GFAs but also possess highly complex structures. In this section, MCMGs are roughly divided into three groups by shape: high mixing entropy BMGs, MCMG films, and MC amorphous micro-fibers. Although their processing routes are not completely the same, MCMGs in each group have similar forming conditions.

4.1. High-entropy BMGs

Although BMGs have been studied for several decades, the effect of high-entropy is a relatively new research focus. In 2002, several equal or near-equal atomic BMGs

were designed to secure high GFA and novel properties. Ma *et al.*,[46] for example, synthesized a series of novel MCAs $Ti_{20}Zr_{20}Hf_{20}Cu_{20}M_{20}$ (M = Fe, Co, Ni), in which the concentration of each element is 20 at%. In addition to the equal atomic ratio, the selection of the elements is well in accordance with the three empirical rules described above. The same research team discovered equal-atomic $Ti_{20}Zr_{20}Cu_{20}Ni_{20}Hf_{20}$BMG with critical diameter of 1.5 mm, which is known as the first reported high-entropy BMG. Cantor *et al.*[47] designed a series of novel MCAs by equal atomic substitution in the same year, and produced stable $(Ti_{33}Zr_{33}Hf_{33})_{40}(Ni_{50}Cu_{50})_{50}Al_{10}$ amorphous alloy ribbons via melt spinning; the alloy cannot be strictly defined as a BMG (20–30 μm thick), however. Subsequently, Chen *et al.*[48] designed a septenary $Cu_{0.5}$NiAlCoCrFeSi alloy, which is almost entirely amorphous but a little BCC structure. Besides, the alloy has a comparable corrosion resistance to type-304 stainless steel.

The aforementioned confusion principle (i.e., heightened complexity of components,) formed the design strategy of the above alloys. After the above studies, this type of MGs fell out of popularity in the research community for some time until 2011, when Gao *et al.*[50] reported $Sr_{20}Ca_{20}Yb_{20}Mg_{20}Zn_{20}$, $Sr_{20}Ca_{20}Yb_{20}Mg_{20}Zn_{10}Cu_{10}$, $Sr_{20}Ca_{20}Yb_{20}(Li_{0.55}Mg_{0.45})_{20}Zn_{20}$ as high mixed-entropy BMGs with unique physical and mechanical properties. HE-BMGs then emerged as a popular concept in the literature.

Besides equal or near-equal atomic ratio, it is necessary for HE-BMGs to have sufficiently large GFA to form bulk shape – this is the characteristic primarily distinguishing them from other types of MCAs. As a notable example, Ding *et al.*[7] reported $Ti_{20}Zr_{20}Cu_{20}Ni_{20}Be_{20}$ with critical diameter of 3 mm. The GFA of the alloy is far less than vit-1 discovered by Johnson,[22] although they have similar elements. After adding Hf as the sixth principal element,[8] senary $Ti_{16.7}Zr_{16.7}Hf_{16.7}Cu_{16.7}Ni_{16.7}Be_{16.7}$HE-BMG reaches the critical diameter of 15 mm, i.e., the optimal GFA reported in equal-atomic BMGs to date. Recent researchers[10] have developed Ni-free $Ti_{20}Zr_{20}Hf_{20}Be_{20}Cu_{20}$ BMG with critical diameter of 12 mm, which is the largest size in reported quinary HE-BMGs.

Chen *et al.*[9] considered that a large component number can make up for the decreasing entropy caused by an unequal atomic ratio, and designed nine-component, non-equal atomic $Zr_{40}Hf_{10}Ti_4Y_1Al_{10}Cu_{25}Ni_7Co_2Fe_1$BMG accordingly; its critical diameter can reach centimeter-level (12 mm).

As a special group of BMGs, rare earth-based BMGs exhibit a number of exciting properties. For example, the T_g of $Ce_{70}Al_{10}Cu_{20}$ and $Ce_{68}Al_{10}Cu_{20}Nb_2$BMGs is close to that of some polymers.[55] The Nb–Fe–Al alloy system has hard magnetic properties at room temperature.[56,57] $Gd_{53}Al_{24}Co_{20}Zr_3$ and $Gd_{51}Al_{24}Co_{20}Zr_4Nb_1$ BMGs have giant magneto-caloric effects and would be the potential candidates for magnetic refrigerants.[57] He *et al.* reported equal atomic HE-BMGs of $Gd_{20}Tb_{20}Dy_{20}Al_{20}M_{20}$ (M = Fe, Co, Ni)[51] and $Ho_{20}Er_{20}Co_{20}Al_{20}RE_{20}$ (RE = Gd, Dy, Tm),[52] which have several principle elements of RE. The materials also exhibit excellent magneto-caloric properties and the refrigerant capacity of $Ho_{20}Er_{20}Co_{20}Al_{20}Gd_{20}$ can reach 627 J·kg^{-1} at 5 T – considerably larger than most rare earth-based BMGs.

It is known that several biomedical BMGs, such as Ti-based, Zr-based, and Fe-based BMGs, possess a favorable combination of excellent mechanical properties and corrosion resistance.[58] Chen *et al.*[59] reported the high general corrosion resistance of seven-component $Cu_{0.5}$NiAlCoCrFeSi BMGs in boiling water, which suggests the potential application of HE-BMGs in corrosive environments. Biocompatibility is another essential factor for biomaterials. Braic *et al.*[60] investigated the biocompatibility of MC film (TiZrNbHfTa)N and (TiZrNbHfTa)C and found that they did not stimulate any cytotoxic response by osteoblasts after 24 h and 72 h, respectively. These films form an FCC solid solution instead of an amorphous phase, however. Whether MCMG films have comparable biocompatibility merits further research.

Table 1 summarizes the HE-BMGs reported from 2002 until now, where the atomic substitution of typical BMGs appears to be a common approach.[61] For example, $Ti_{20}Zr_{20}Cu_{20}Ni_{20}Be_{20}$ was developed from $Zr_{41.2}Cu_{12.5}Ni_{10}Ti_{13.8}Be_{22.5}$ by adjusting the atomic ratio to equal. $Pd_{20}Pt_{20}Cu_{20}Ni_{20}P_{20}$[49] and $Y_{56-x}M_xAl_{24}Co_{20}$ (M = Ce, Pr, Nd)[54] were respectively developed from $Pd_{40}Ni_{40}P_{20}$ and $Y_{56}Al_{24}Co_{20}$ by replacing several elements. The difference between non-equal atomic HE-BMG and conventional BMGs is practically negligible, however. The HE-BMG concept provides a new perspective from which the research community can rediscover these alloys.

Table 1. HE-BMGs reported to date.

Composition	d_c/mm	Year
Equal atomic HE-BMGs		
$Ti_{20}Zr_{20}Cu_{20}Ni_{20}Hf_{20}$[46]	1.5	2002
$Ti_{20}Zr_{20}Cu_{20}Ni_{20}Be_{20}$[7]	3	2013
$Ti_{16.7}Zr_{16.7}Cu_{16.7}Ni_{16.7}Be_{16.7}$ $Hf_{16.7}$[8]	> 15	2014
$Ti_{20}Zr_{20}Cu_{20}Be_{20}Hf_{20}$[10]	12	2015
$Pd_{20}Pt_{20}Cu_{20}Ni_{20}P_{20}$[49]	10	2011
$Al_{20}Er_{20}Dy_{20}Ni_{20}Tb_{20}$[50]	2	2011
$Sr_{20}Ca_{20}Yb_{20}Mg_{20}Zn_{20}$[50]	2×5 mm^2 (plates)	2011
$Gd_{20}Tb_{20}Dy_{20}Al_{20}M_{20}$ (M = Co, Ni)[51]	1	2015
$Ho_{20}Er_{20}Co_{20}Al_{20}RE_{20}$ (RE = Gd, Dy, Tm)[52]	1	2015
Near equal atomic HE-BMGs		
$Sr_{20}Ca_{20}Yb_{20}Mg_{20}Zn_{10}Cu_{10}$[50]	5	2011
$Sr_{20}Ca_{20}Yb_{20}(Li_{0.55}Mg_{0.45})_{20}Zn_{20}$[50]	3	2011
$Cu_{0.5}$NiAlCoCrFeSi[53]	3	2005
$Y_{56-x}M_xAl_{24}Co_{20}$ (M = Ce, Pr, Nd; x = 5, 10, 15, 20 at%)[54]	–	2012
Non-equal atomic HE-BMGs		
$Zr_{40}Hf_{10}Ti_4Y_1Al_{10}Cu_{25}Ni_7Co_2Fe_1$[9]	14	2015

4.2. Multi-component metallic-glass films

MCMG films are typically deposited on steel or Si substrates in argon or nitrogen atmosphere and are thinner than ribbons fabricated via melt spinning route. One of the more important influence factors on phase formation is the sluggish diffusion effect caused by high mixing entropy in MCMG films, which endows MCMG films with good thermal stability.[3] The MCMG film formation process is also related to the transformation from ionic state to solid state, which causes considerably high cooling rate; to this effect, kinetics factors dominate the phase formation (compared to cast MCMGs).[62]

Because the forming conditions of MCMG films deviate from thermodynamic equilibrium, the methods based on thermodynamic parameter can probably predict the trend of phase formation in MCMG films, which is not comparable with HE-BMGs. After taking kinetic factors into account, molecular dynamics simulation indicates that Ω and δ can effectively predict the evolution from solid solution to amorphous phase in AlCoCrCuFeNi thin film.[63]

Table 2. MCMG films reported to now.

MCMG films		MCMG nitride films	
Composition	Year	Composition	Year
AlCrTaTiZr[64]	2006	$AlCrTaTiZrN_x$[64]	2006
TiAlCrSiV[65]	2007	$(TiAlCrSiV)_{53.8}N_{46.2}$[65]	2007
AlMoNbSiTaTiVZr[66]	2008	$(AlMoNbSiTaTiVZr)N_x$[66]	2008
NbSiTaTiZr[67]	2009	–	–
AlCrTaTiZrRu[68]	2011	–	–
AlCrSiTiZr[69]	2012	–	–
AlBCrSiTi[70]	2012	AlBCrSiTiN[70]	2012
NbTiAlSiW[71]	2016	$NbTiAlSiW_xN_y$[71]	2016

Another type of MCMG films is deposited in nitrogen atmosphere to form nitride films with high high hardness and excellent wear resistance. The effects of nitrogen on phase formation differ across various alloy systems. Under the confusion principle,[27] the addition of nitrogen raises the complexity of the system, thus contributing to the GFA of the MCMG films. Chen *et al.*[3] confirmed this in their study on FeCoNiCrCuAlMn and $FeCoNiCrCuAl_{0.5}$ films. As the nitrogen flow ratio increases, the crystallinity of the nitride films decreases and finally an amorphous phase is formed. As an example,[71] figure 6 shows the XRD patterns of $NbTiAlSiN_y$ films under different formation and annealing conditions. The diffraction intensity gradually decreases as the N_2 flow rate increases (Fig. 6(a)). Moreover, the films retain excellent thermal stability and do not exhibit any obvious crystallization under 700 °C for 24 h, as shown in Fig. 6(b). Thus, $NbTiAlSiN_y$ films have promising applications in high-temperature environments. Amorphous structure is easier to form at lower nitrogen content in AlCrTaTiZr nitride film, however.[64] Similar tendencies have been observed in TiAlCrSiV,[65] AlMoNbSiTaTiVZr,[66] and AlCrSiTiZr[69] nitride films as well. These phenomena indicate that excessive nitrogen causes nanostructure nitrides to form, where the hardness of the films is normally improved. The MCMG films reported to date are summarized in Table 2.

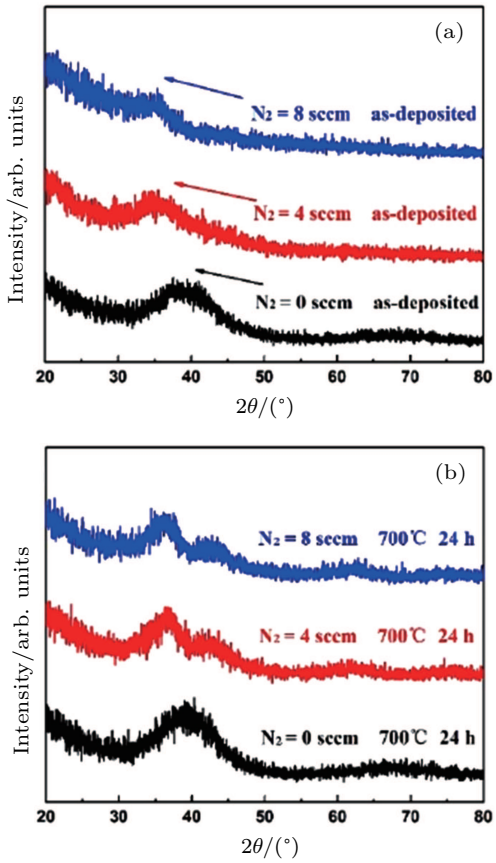


Fig. 6. (color online) XRD patterns of NbTiAlSiWNy film before and after heat-treatment: (a) as-deposited; (b) 700 °C for 24 h. The figure is reproduced from Ref. [71].

4.3. GMI effect of multi-component amorphous micro-fibers

MC amorphous micro-fibers are small-sized MCMGs which satisfy micro device application requirements. They are normally obtained by the melt spinning method. Certain ferromagnetic amorphous micro-fibers possess excellent soft magnetic properties and have attractive potential in regards to magnetic sensor application. Although several ferromagnetic HEAs exhibit outstanding magnetic properties, most also possess crystal structure,[72] which results in magnetic anisotropy. For instance, the coercivity of non-equal atomic $FeCoNiAl_{0.2}Si_{0.2}$ HEA is greatly influenced by the crystal orientation and grain size of the alloy. This notable magnetic anisotropy induced by crystal structure can be effectively eliminated in MC amorphous micro-fibers.

The giant magneto-impedance (GMI) effect in $Co_{68.15}Fe_{4.35}Si_{12.5}B_{15}$ amorphous micro-fiber was first discovered by Mohri,[73] who found that the impedance of the micro-fiber can be dramatically changed under the applied

magnetic field. Subsequently, GMI effect has also been found in amorphous ribbons[74,75] and multilayer films.[76,77] The origin of the GMI effect is normally explained by the skin effect of the conductor under high frequency. In ferromagnetic amorphous micro-fibers, domain wall movement is affected by the external magnetic field, and the skin depth is dependent on the circumferential permeability, which changes as the circular domain wall moves.[78]

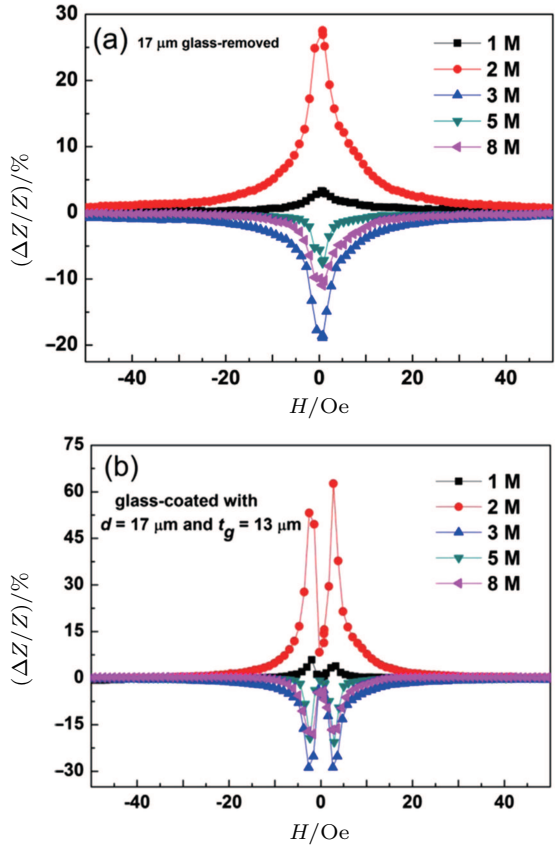


Fig. 7. (color online) GMI ratio for (a) glass-removed micro-fiber with diameter of 17 mm and (b) glass-coated micro-fiber with metallic nucleus diameter of 17 mm and glass thickness of 13 mm. The figure is reproduced from Ref. [79].

The GMI effect of the micro-fiber can be improved by controlling the processing method, applied stress, and heat treatment, among other approaches. As an example, the GMI ratio $(\Delta Z/Z)$ of glass-coated and glass-removed $Co_{69.5}Fe_{4.35}Cr_1Si_8B_{17}$ amorphous fibers with similar diameter is shown in Fig. 7.[79] The GMI ratio curve transforms from a single peak to double peaks due to the different surface magnetic anisotropy characteristics of the fibers.

Another effective way to adjust the GMI effect is to make several soft magnetic amorphous fibers into a bundled amorphous-fiber composite. Compared to a single amorphous micro-fiber, multi-strand amorphous fibers have various responses to the external field, which is due to the dipolar interaction among the fibers. This interaction not only alters the hysteresis loop of the fibers,[80] but also has considerable impact on the GMI behavior. Sinnecker *et al.*[81] placed annealed $Fe_{77.5}Si_{7.5}B_{15}$ amorphous fibers on the side of $Co_{70}Fe_5Si_{15}B_{10}$ amorphous fibers and found that the GMI ratio of $Co_{70}Fe_5Si_{15}B_{10}$ amorphous fibers is asymmetrical from the positive to negative field. García *et al.*[82] investigated the GMI effect of a micro-fiber array involving various quantities of amorphous fibers, and found that the relationship between GMI ratio and number of fibers is also associated with the frequency.

4.4. Further development of multi-component metallic-glasses

In terms of thermodynamics, MCMGs represent an important opportunity to explore the effects of high mixed entropy on phase formation and non-crystalline structure. From the perspective of BMG design, strategies for fabricating MCMGs offer an opportunity to discover novel amorphous phase-forming compositions from the center of relevant diagrams. The properties of the principle elements can be magnified via "cocktail effect", in which the minor additional elements are deliberately not comparable. As a departure from the typical BMGs, the favorable or even optimal properties can be obtained in MCMGs. For instance, (AlBCrSiTi)N MCMG nitride films exhibit strong glass formability at high temperatures, which is closely related to the sluggish diffusion effect of multi-elements.[70] $Cu_{0.5}$NiAlCoCrFeSi retains good mechanical properties and excellent corrosion resistance in boiling water.[53,59] HEAs, which has high irradiation resistance, can be used in nuclear reactors,[11,12] and certain Zr-based and Ti-based BMGs have many potential applications in the biomaterials field.[58] Certainly, novel MCMGs will continue to be a worthwhile research object in the future.

5. Conclusion

Recent studies on amorphous phase formation in MCAs and novel MCMGs were reviewed and summarized in this paper. The literature suggests that amorphous phase formation is greatly impacted by the parameters Ω, ΔH_{mix}, ΔS_{mix}, δ and $\langle \varepsilon^2 \rangle^{1/2}$. Diagrams established by these parameters are normally used to identify MCA phase formation. Further, a number of MCMGs have been developed based on typical BMGs via atomic substitution in recent decades. Most resulting materials show excellent GFA, and some do not strictly corresponding to the amorphous phase formation rules. MCMG films with good thermal stability have promising applications in high-temperature environments, and the GMI effect of MC amorphous micro-fibers is well-suited to the magnetic sensor field.

In short, MCAs merit further research by virtue of their remarkable potential in a variety of applications. By the design strategies of MCA, the structure and formation of BMGs can be understood from an innovative perspective. It is reasonable

to expect that coming years will see new types of BMGs with remarkable properties.

References

[1] Ranganathan S 2003 *Curr. Sci.* **85** 1404
[2] Yeh J W, Chen S K, Lin S J, Gan J Y, Chin T S, Shun T T, Tsau C H and Chang S Y 2004 *Adv. Eng. Mater.* **6** 299
[3] Chen T K, Shun T T, Yeh J W and Wong M S 2004 *Surf. Coat. Tech.* **188–189** 193
[4] Wang X F, Zhang Y, Qiao Y and Chen G L 2007 *Intermetallics* **15** 357
[5] Pradeep K G, Tasan C C, Yao M J, Deng Y, Springer H and Raabe D 2015 *Materials Science and Engineering: A* **648** 183
[6] Ma D, Yao M, Pradeep K G, Tasan C C, Springer H and Raabe D 2015 *Acta Mater.* **98** 288
[7] Ding H Y and Yao K F 2013 *J. Non-Cryst. Solids* **364** 9
[8] Ding H Y, Shao Y, Gong P, Li J F and Yao K F 2014 *Mater. Lett.* **125** 151
[9] Chen C, Pang S, Cheng Y and Zhang T 2015 *J. Non-Cryst. Solids* **410** 39
[10] Zhao S F, Yang G N, Ding H Y and Yao K F 2015 *Intermetallics* **61** 47
[11] Xia S Q, Yang X, Yang T F, Liu S and Zhang Y 2015 *Jom-Us* **67** 2340
[12] Xia S, Gao M C, Yang T, Liaw P K and Zhang Y 2016 *J. Nucl. Mater.* **480** 100
[13] Inoue A and Takeuchi A 2005 *Mater. Trans.* **46** 2817
[14] Klement W, Willence R H and Duwez P 1960 *Nature* **187** 869
[15] Guo S 2015 *Mater. Sci. Tech. Lond.* **31** 1223
[16] Murty B S, Yeh J W and Ranganathan S 2014 *High-Entropy Alloys* (Elsevier Inc. online) pp. 37–56
[17] Turnbull D 1969 *Contemp. Phys.* **10** 473
[18] Inoue A, Nakamura T, Nishiyama N and Masumoto T 1992 *Mater. Trans.* **33** 937
[19] Inoue A, Zhang T, Nishiyama N, Ohba K and Masumoto T 1993 *Mater. Trans.* **34** 1234
[20] Inoue A, Zhang T and Masumoto T 1995 *Mater. Trans.* **36** 391
[21] Inoue A, Nakamura T and Matsuda T 1996 *Mater. Trans.* **37** 181
[22] Peter A and Johnson W L 1993 *Appl. Phys. Lett.* **63** 2342
[23] Lou H B, Wang X D, Xu F, Ding S Q and Cao Q P 2011 *Appl. Phys. Lett.* **99** 051910
[24] Inoue A 2000 *Acta Mater.* **48** 279
[25] Inoue A, Zhang T and Masumoto T 1993 *J. Non-Cryst. Solids* **156–158** 473
[26] Lu Z P and Liu C T 2002 *Acta Mater.* **50** 3501
[27] Greer L 1993 *Nature* **366** 303
[28] Cantor B, Chang I T H, Knight P and Vincent A J B 2004 *Materials Science and Engineering: A* **375–377** 213
[29] Zhou Y J, Zhang Y, Wang Y L and Chen G L 2007 *Appl. Phys. Lett.* **90** 181904
[30] Takeuchi A, Amiya K, Wada T, Yubuta K and Zhang W 2014 *Jom-Us* **66** 1984
[31] Zhang Y, Zuo T T, Tang Z, Gao M C, Dahmen K A, Liaw P K and Lu Z P 2014 *Prog. Mater. Sci.* **61** 1
[32] Takeuchi A and Inoue A 2001 *Materials Science and Engineering: A* **304–306** 446
[33] Senkov O N and Miracle D B 2001 *Mater. Res. Bull.* **36** 2183
[34] Takeuchi A, Amiya K, Wada T, Yubuta K, Zhang W and Makino A 2013 *Entropy-Switz* **15** 3810
[35] Xia M, Zhang S, Ma C and Li J 2006 *Appl. Phys. Lett.* **89** 91917
[36] Yang X and Zhang Y 2012 *Mater. Chem. Phys.* **132** 233
[37] Zhang Y, Zhou Y J, Lin J P, Chen G L and Liaw P K 2008 *Adv. Eng. Mater.* **10** 534
[38] Guo S, Hu Q, Ng C and Liu C T 2013 *Intermetallics* **41** 96
[39] Wang Z, Guo S and Liu C T 2014 *Jom-Us* **66** 1966
[40] Egami T 1997 *Materials Science and Engineering: A* **226–228** 261
[41] Egami T 2011 *Prog. Mater. Sci.* **56** 637
[42] Ye Y F, Liu C T and Yang Y 2015 *Acta Mater.* **94** 152
[43] Takeuchi A, Wang J, Chen N, Zhang W, Yokoyama Y, Yubuta K and Zhu S 2013 *Mater. Trans.* **54** 776
[44] Yang X, Chen S Y, Cotton J D and Zhang Y 2014 *Jom-Us* **66** 2009
[45] Guo S and LIU C T 2011 *Progress in Natural Science: Materials International* **21** 433
[46] Ma L, Wang L, Zhang T and Inoue A 2002 *Mater. Trans.* **43** 277
[47] Cantor B, Kim K B and Warren P J 2002 *Materials Science Forum* **386–388** 27
[48] Chen Y Y, Duval T, Hung U D, Yeh J W and Shih H C 2005 *Corros. Sci.* **47** 2257
[49] Takeuchi A, Chen N, Wada T, Yokoyama Y, Kato H, Inoue A and Yeh J W 2011 *Intermetallics* **19** 1546
[50] Gao X Q, Zhao K, Ke H B, Ding D W, Wang W H and Bai H Y 2011 *J. Non-Cryst. Solids* **357** 3557
[51] Huo J, Huo L, Men H, Wang X, Inoue A, Wang J, Chang C and Li R 2015 *Intermetallics* **58** 31
[52] Huo J, Huo L, Li J, Men H, Wang X, Inoue A, Chang C, Wang J and Li R 2015 *J. Appl. Phys.* **117** 73902
[53] Chen Y Y, Hong U T, Yeh J W and Shih H C 2005 *Appl. Phys. Lett.* **87** 261918
[54] He S W 2012 *Applied Mechanics and Materials* **268–270** 301
[55] Zhang B, Zhao D Q, Pan M X, Wang W H and Greer A L 2005 *Phys. Rev. Lett.* **94** 205502
[56] Inoue A, Zhang T, Zhang W and Takeuchi A 1996 *Mater.Trans.* **37** 99
[57] Luo Q and Wang W H 2009 *J. Non-Cryst. Solids* **355** 759
[58] Li H F and Zheng Y F 2016 *Acta Biomater.* **36** 1
[59] Chen Y Y, Duval T, Hong U T, Yeh J W, Shih H C, Wang L H and Oung J C 2007 *Mater. Lett.* **61** 2692
[60] Braic V, Balaceanu M, Braic M, Vladescu A, Panseri S and Russo A 2012 *J. Mech. Behav. Biomed.* **10** 197
[61] Gao M C, Yeh J, Liaw P K and Zhang Y 2016 *High-Entropy Alloys* (Springer International Publishing)
[62] Guo S, Hu Q, Ng C and Liu C T 2013 *Intermetallics* **41** 96
[63] Xie L, Brault P, Thomann A, Yang X, Zhang Y and Shang G 2016 *Intermetallics* **68** 78
[64] Lai C, Lin S, Yeh J and Chang S 2006 *Surf. Coat. Tech.* **201** 3275
[65] Lin C H, Duh J G and Yeh J W 2007 *Surf. Coat. Tech.* **201** 6304
[66] Tsai M, Lai C, Yeh J and Gan J 2008 *J. Phys. D: Appl. Phys.* **41** 235402
[67] Yang T, Huang R, Wu C, Chen F, Gan J, Yeh J and Narayan J 2009 *Appl. Phys. Lett.* **95** 241905
[68] Chang S, Wang C, Chen M and Li C 2011 *J. Alloy. Compd.* **509** L85
[69] Hsueh H, Shen W, Tsai M and Yeh J 2012 *Surf. Coat. Tech.* **206** 4106
[70] Tsai C, Lai S, Cheng K, Tsai M, Davison A, Tsau C and Yeh J 2012 *Thin Solid Films* **520** 2613
[71] Sheng W, Yang X, Wang C and Zhang Y 2016 *Entropy-Switz* **18** 226
[72] Zuo T T, Li R B, Ren X J and Zhang Y 2014 *J. Magn. Magn. Mater.* **371** 60
[73] Mohri K, Kohzawa T and Kawashima K 1992 *IEEE T. Magn.* **28** 3150
[74] Knobel M, Chiriac H, Sinnecker J P, Marinescu S, Óvári T A and Inoue A 1997 *Sensors and Actuators A: Physical* **59** 256
[75] Chiriac H, Vinai F, Óvári T A, Malinesen C S, Barariu F and Tiberto P 1997 *Materials Science and Engineering: A* **226–228** 646
[76] Da Silva R B, Silva E F, Mori T J A, Della Pace R D, Dutra R, Corrêa M A, Bohn F and Sommer R L 2015 *J. Magn. Magn. Mater.* **394** 87
[77] García-Arribas A, Fernández E, Svalov A, Kurlyandskaya G V and Barandiaran J M 2016 *J. Magn. Magn. Mater.* **400** 321
[78] Panina L V and Mohri K 1994 *Appl. Phys. Lett.* **65** 1189
[79] Zhao Y, Hao H and Zhang Y 2013 *Intermetallics* **42** 62
[80] Sampaio L C, Sinnecker E H C P, R C C G, Knobel M, Vazquez M and Velazquez J 2000 *Phys. Rev. B* **61** 8976
[81] Sinnecker J P, de Araujo A E P, Piccin R, Knobel M and Zquez M V 2005 *J. Magn. Magn. Mater.* **295** 121
[82] García C, Zhukova V, Zhukov A, Usov N, Ipatov M, Gonzalez J and Blanco J M 2007 *Sensor Lett.* **5** 10